Translational Science

Cancer Research

BET Inhibition Overcomes Receptor Tyrosine Kinase–Mediated Cetuximab Resistance in HNSCC

Brandon Leonard, Toni M. Brand, Rachel A. O'Keefe, Eliot D. Lee, Yan Zeng, Jacquelyn D. Kemmer, Hua Li, Jennifer R. Grandis, and Neil E. Bhola

Abstract

Cetuximab, the FDA-approved anti-EGFR antibody for head and neck squamous cell carcinoma (HNSCC), has displayed limited efficacy due to the emergence of intrinsic and acquired resistance. We and others have demonstrated that cetuximab resistance in HNSCC is driven by alternative receptor tyrosine kinases (RTK), including HER3, MET, and AXL. In an effort to overcome cetuximab resistance and circumvent toxicities associated with the administration of multiple RTK inhibitors, we sought to identify a common molecular target that regulates expression of multiple RTK. Bromodomain-containing protein-4 (BRD4) has been shown to regulate the transcription of various RTK in the context of resistance to PI3K and HER2 inhibition in breast cancer models. We hypothesized that, in HNSCC, targeting BRD4 could overcome cetuximab resistance by depleting alternative RTK expression. We generated independent models of cetuximab resistance in HNSCC cell lines and interrogated their RTK and BRD4 expression profiles. Cetuximab-resistant clones displayed increased expression and activation of several RTK, such as MET and AXL, as well as an increased percentage of BRD4-expressing cells. Both genetic and pharmacologic inhibition of BRD4 abrogated cell viability in models of acquired and intrinsic cetuximab resistance and was associated with a robust decrease in alternative RTK expression by cetuximab. Combined treatment with cetuximab and bromodomain inhibitor JQ1 significantly delayed acquired resistance and RTK upregulation in patient-derived xenograft models of HNSCC. These findings indicate that the combination of cetuximab and bromodomain inhibition may be a promising therapeutic strategy for patients with HNSCC.

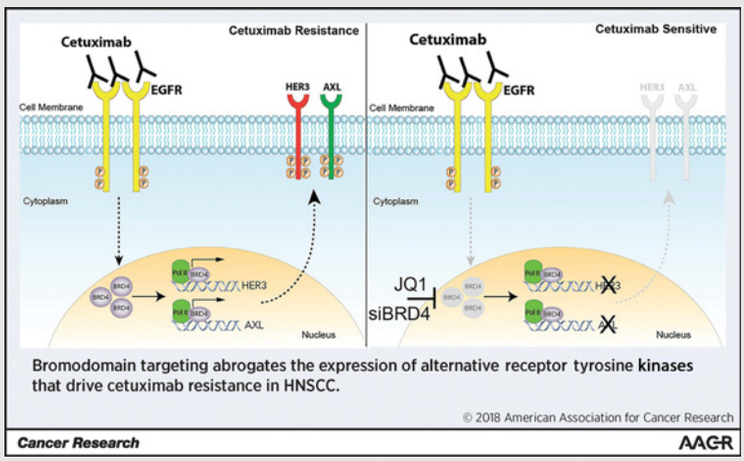

Significance: Inhibition of bromodomain protein BRD4 represents a potential therapeutic strategy to circumvent the toxicities and financial burden of targeting the multiple receptor tyrosine kinases that drive cetuximab resistance in HNSCC and NSCLC.

Graphical Abstract: http://cancerres.aacrjournals.org/content/canres/78/15/4331/F1.large.jpg. *Cancer Res; 78(15); 4331–43. ©2018 AACR.*

Introduction

Nearly 600,000 people are diagnosed annually with head and neck cancer worldwide and 60% succumb to their disease within 5 years (1). The EGFR was discovered to be a major driver of HNSCC and, in 2006, the EGFR mAb cetuximab was FDA-approved for HNSCC treatment (2). Unfortunately, cetuximab has not conferred significant long-term benefit due to treatment resistance. Mechanisms underlying resistance to EGFR blockade in multiple cancer types have been a major focus of investigations aimed at improving the durability of response to cetuximab and other clinically approved EGFR inhibitors (3–5). Cumulative evidence implicates upregulation and activation of multiple receptor tyrosine kinases (RTK) mediating resistance to cetuximab in HNSCC (6–8). In addition, RTKs have been shown to mediate cetuximab resistance in models of lung and colon cancer (9, 10). These upregulated receptors have been shown to individually drive rapid growth and poor differentiation, and thereby circumvent the antitumor effects of cetuximab (11). Several studies have

Department of Otolaryngology and Head and Neck Surgery, University of California San Francisco, San Francisco, California.

Note: Supplementary data for this article are available at Cancer Research Online (http://cancerres.aacrjournals.org/).

Corresponding Author: Neil E. Bhola, University of California San Francisco, 1450 3rd Street, HD213, San Francisco, CA 94158. Phone: 415-502-3638; Fax: 415-514-8520; E-mail: Neil.bhola@ucsf.edu

doi: 10.1158/0008-5472.CAN-18-0459

demonstrated that treatment with at least two RTK inhibitors is needed to mitigate cetuximab resistance (10). To avoid the likely toxicity and prohibitive costs associated with administration of multiple RTK inhibitors in combination with cetuximab, we sought to identify and target a common mechanism that regulates the expression of these receptors.

A recent study showed that resistance to the HER2 inhibitor lapatinib can be mediated by increased RTK expression in models of HER2-positive breast cancer. The authors discovered that RTK expression was dependent on the bromodomain and extra terminal protein BRD4 (12). In parallel, another group found that RTK upregulation can also drive resistance to PI3K inhibition in breast cancer. Bromodomain inhibition was shown to diminish RTK upregulation and enhance the antitumor efficacy of PI3K blockade (13). On the basis of these observations, we hypothesized that blockade of BRD4 will overcome cetuximab resistance in HNSCC by inhibiting upregulation and activation of alternative RTKs.

BRD4 is a member of the bromodomain and extra terminal (BET) protein family. BRD4 is characterized by the expression of two bromodomain regions, an extra terminal region, and a C-terminal domain (14). BET family proteins bind to acetylated lysines found on chromatin or certain proteins via conserved bromodomain regions. Recruitment of BRD4 to acetylated lysines on chromatin facilitates recruitment and activation of CDK9, which is part of the P-TEFB complex. RNA polymerase II is then phosphorylated and is subsequently capable of initiating gene transcription (15, 16). The ability of BET family members, particularly BRD4, to influence chromatin state has made it an attractive therapeutic target in recent years and inhibitors against bromodomains have demonstrated promising antitumor efficacy in preclinical models (17–19).

In this study, we demonstrate that HNSCC preclinical models of cetuximab resistance express a heterogeneous milieu of activated RTKs, which are driven in part by BRD4. In addition, analysis of a cohort of patients with cetuximab-treated HNSCC with progression-free survival lower than 5.6 months indicated increased expression of RTKs such as AXL and ROR2. Genetic or pharmacologic inhibition of BRD4 sensitizes resistant cells to cetuximab and abrogates the regrowth of cetuximab-treated HNSCC patient-derived xenografts (PDX) by preventing the upregulation of the alternative RTKs that drive cetuximab resistance. These studies highlight the need to evaluate the clinical efficacy of bromodomain inhibitors in HNSCC.

Materials and Methods

Cell lines and reagents

All cell lines were cultured in DMEM (MediaTech Inc), 10% FBS (Gemini Bioproducts) and 1% penicillin–streptomycin (Life Technologies). FaDu, CAL27, SCC4, and SCC9 cells were obtained from ATCC. PECAPJ49 cells were purchased from Sigma-Aldrich. CAL33 cells were provided by Gerard Milano (University of Nice, Nice, France). The H226 parental (HP) and cetuximab-resistant clones (HC1, HC4, HC8) were provided by Deric Wheeler (University of Wisconsin, Madison, WI). UM-SCC47 cells were provided by Thomas Carey (University of Michigan, Ann Arbor, MI). HSC-6 cells were obtained from Johji Inazawa (Tokyo Medical and Dental University, Tokyo, Japan). Spontaneously immortalized normal oral keratinocytes (NOKsi) were provided by Nevan Krogan (University of California San Francisco, San Francisco, CA). All cell lines were authenticated every 6 months during the course of experiments via short-tandem repeat testing (Genetica DNA Laboratories). *Mycoplasma* testing was not performed during the course of this study. Cell lines were passaged for a period of 3 months (~24 passages) after thawing from liquid nitrogen. PECAPJ49 vector and HER3-expressing lines were generated as described previously (20).

JQ1 was provided by Dr. James Bradner (Dana-Farber Cancer Institute, Boston, MA) for *in vitro* studies. JQ1 for *in vivo* experiments was obtained from APExBIO and dissolved in 10% cyclodextrin (Sigma-Aldrich #H107). I-BET-762 was obtained from Selleckchem. MZ1 was purchased from Tocris Bioscience.

Generation of cetuximab-resistant cell lines

To generate cetuximab-resistant models, PECAPJ49, FaDu, and CAL33 cells were treated with a concentration of cetuximab, which resulted in approximately 50% survival. The cells treated with cetuximab were then cultured at 20% confluency in the presence of 100 nmol/L cetuximab for 1–2 weeks. Four surviving colonies from the cetuximab-treated plates were selected using cloning rings and labeled as CTXR#1, #2, etc. Parental cells were passaged alongside the clones under cetuximab selection pressure. Selected clones were cultured with increasing cetuximab concentrations (150, 200, 300, and 500 nmol/L) every 2–3 weeks. Cetuximab response was evaluated by a 96-hour crystal violet viability assay following treatment with 100 nmol/L cetuximab after 3, 4, 5, and 6 months.

Flow cytometry

Parental and cetuximab-resistant clones were plated in 60-mm dishes and cultured at 37°C. After 72 hours, cells were trypsinized and counted. An equal number of viable cells were fixed and permeabilized using the True Nuclear Transcription Factor Buffer Set (BioLegend), and then stained with anti-BRD4 (Abcam #ab128874; 1:400) for 15 minutes. Cells were then stained with an AlexaFluor 488 secondary antibody (Life Technologies #11008; 1:500) for 15 minutes in the dark, washed in FACS buffer, and analyzed using the FACSCalibur. Samples stained with only the FITC secondary antibody was used to account for background and to set the gate for BRD4-positive cells. The percentage of BRD4-positive cells was quantified using the FlowJo Software. For EGFR staining, cells were stained with EGFR-Alexa Fluor 488 antibody (Biolegend #352907; 1:200) for 15 minutes in the dark at room temperature. Cells were then washed once and resuspended in FACS buffer and then analyzed. Quantification was performed using FlowJo software.

DNA pull-down assay

Cytoplasmic and nuclear extracts from PECAPJ49 parental and CTXR#4 cells were obtained using the described protocol (21). The DNA pull-down protocol was modified from the described protocol (22). Two-hundred micrograms of cytoplasmic and nuclear lysate was incubated with 2 μg of annealed AXL promoter or scrambled biotinylated oligonucleotides (Sigma-Aldrich) and 30 μL of streptavidin-coupled magnetic Dynabeads (Thermo Scientific) for two hours at room temperature. The sequence of the biotinylated AXL promoter oligonucleotide used was: 5′-[Btn]GGCTCAGGAGGCCAGTCACTTGCCTGTAGCCCACAGTT-AGTGGTAGCACTGGGATTCCAACTTGGGTCCCCTTCATGTCG-CCTGTATTTGGTGTCCCATTTAGGCGTCCATGCAGGTTTT-3′. The sequence manipulation suite (http://www.bioinformatics.org/sms2/shuffle_dna.html) was used to generate the scrambled oligonucleotide. Streptavidin-biotin–bound lysate was

washed with 0.5% NP-40 buffer four times in a magnetic rack. Lysate was then resuspended in sample buffer and boiled for three minutes, resolved by SDS-PAGE, and probed for BRD4 and phospho-CDK9.

Chromatin immunoprecipitation assay

PECAPJ49 parental and CTXR#4 cells were cultured to 60% confluency and treated with vehicle or 300 nmol/L JQ1 for 72 hours. The Magna-ChIP Chromatin Immunoprecipitation Kit (Millipore) was used to perform chromatin immunoprecipitation (ChIP). Cells were washed with PBS and then crosslinked with 1% formaldehyde for 10 minutes and then quenched with 125 mmol/L glycine. Cell pellets were then lysed according to the Magna-ChIP protocol. Chromatin was sonicated using optimized conditions. Sheared chromatin was immunoprecipitated with normal IgG (1:500; Millipore, #12-371B), BRD4 (1:100; Active Motif, #39909), and RNA-polymerase II (1:500; Millipore, #05-623B) antibodies. Prior to immunoprecipitation, 1% of the sheared chromatin from each treatment group was removed and used as the input. Antibody complexes were incubated with magnetic protein A/G beads overnight at 4°C. Beads were washed and the protein DNA complexes were eluted with proteinase K and ChIP elution buffer at 62°C in a hybridization oven for 2 hours. DNA was purified according to the Magna-ChIP protocol and prepared for real-time quantitative PCR. PCR reactions were performed using SYBR Green Master Mix and a primer set for the AXL promoter region. AXL promoter primers were: forward, 5′-AGTGGAGTTCTGGAGGAATGTTTAC-3′; reverse, 5′-CTCCTTCCCTCACTCCCAGACT-3′. Fold enrichment was calculated using the formula: BRD4 $[2^{(C_t\text{Input-}C_t\text{IP})}]$/IgG $[2^{(C_t\text{Input-}C_t\text{IP})}]$.

Crystal violet viability assay

Cells were seeded in 96-, 24-, or 6-well dishes and incubated overnight. On the next day, cells were treated with different agents (cetuximab, JQ1, NTC siRNA, BRD4 siRNA, I-BET-762) for 72–96 hours. For clonogenic assays, cells were seeded at low density (200–400 cells/well of 6-well dish) in triplicate and treated with fresh drug every 4 days for a period of 21 days. At the termination of the experiment, cells were stained with crystal violet for 30 minutes. Crystal violet solution was removed from the wells and the plates were washed under tap water before being dried for 24 hours. Crystal violet staining was dissolved with 5% SDS solution and subsequently quantified using a colorimetric plate reader.

Real-time quantitative PCR

RNA was harvested using an RNAeasy Kit (Qiagen) and used to synthesize cDNA (iSCRIPT cDNA Synthesis Kit, Bio-Rad) according to the manufacturer's instructions. PCR reactions were performed using SYBR Green Master Mix (Bio-Rad) and the Bio-Rad CFX96 cycler. Relative mRNA levels were standardized to the housekeeping gene, Tata-binding protein (TBP), mRNA levels.

Immunoblotting and RTK arrays

Cells were washed with ice-cold PBS and then lysed with RIPA lysis buffer (150 mmol/L Tris, pH 7.4, 100 mmol/L NaF, 120 mmol/L NaCl, 100 μmol/L sodium orthovanadate, and 1× protease inhibitor cocktail and phosphatase inhibitor cocktail; Roche). Lysates (30 μg) were resolved by SDS-PAGE and transferred to nitrocellulose membranes, which were incubated with primary antibodies at 4°C overnight or at room temperature for 2 hours, followed by incubation with horseradish peroxidase–conjugated anti-rabbit and anti-mouse secondary antibodies (Bio-Rad) for 1 hour at room temperature. Immunoreactive bands were visualized by chemiluminescence (Santa Cruz Biotechnology). All primary antibodies were from Cell Signaling Technology with the exception of BRD4 (Abcam), Actin (Abcam), and AXL (Life Technologies). For phospho-RTK arrays (R&D Systems), lysates were procured and applied to arrays according to manufacturer's instructions. Arrays were visualized using chemiluminescence. Antibodies used for immunoblotting were from Cell Signaling Technology (P-MET-Y1234 #3126, P-CDK9 #2549, P21 #2947, HER3 #12708, P-HER3-Y1289 #4791, ROR2 #88639, HER2 #2242, P-SFK-Y419 #6943, C-MYC #5605, P-MAPK #9101, GAPDH #5174), Santa Cruz Biotechnology (V5 probe #sc-271944), R&D Systems (P-AXL-Y779 #AF2228, AXL #AF154), Abcam (BRD4 #128874, c-MET #59884, Actin #6276, β-tubulin #6046), and BD Biosciences (EGFR #610016).

RNA interference

Cells were transfected with 50 pmol of siRNA oligonucleotides mixed with Lipofectamine RNAiMAX (Life Technologies). BRD4 siRNA oligonucleotides were obtained through Thermo Scientific. Target sequences for BRD4 siRNAs were: BRD4 siRNA#1: 5′-GGA AAG AGG AAG UGG AAG A-3′, and BRD4 siRNA#2: 5′- GAG AAA GAC AAG AAG GAA A-3′.

PDXs

All animal procedures and maintenance were conducted with protocols approved by the Institutional Animal Care and Use Committee of the University of California, San Francisco (San Francisco, CA; protocol #: AN173372-01C). HNSCC PDXs (6282 and 7157) were established from patients with newly diagnosed HNSCC upon written consent under Institutional review board approval and were established as described previously (23). All PDXs were established in 5- to 6-week-old female NOD.Cg-*Prkdc*^{scid} *Il2rg*^{tm1Wjl}/SzJ (NSG) mice. Once xenografts reached 100 mm^3, mice were randomized to receive vehicle (0.9% normal saline and 10% cyclodextrin), JQ1 (50 mg/kg), cetuximab (20 mg/kg), or the combination with $n = 6$ tumors per treatment group. Cetuximab was administered on days 1 and 5 by intraperitoneal injection. JQ1 was administered 5 days/week by oral gavage. Tumor volume measurements were determined by digital calipers biweekly and calculated using the formula $(\pi)/6 \times$ (large diameter) $\times$ (small diameter)^2. Vehicle and JQ1-treated mice were euthanized at the indicated time points due to visual sign of tumor ulceration. Mice treated with cetuximab or the combination was followed for 37 or 56 days, at which point a significant difference in tumor volumes between the two treatment groups was observed. All tumors were harvested 3 hours after the last treatment for IHC and immunoblot analysis.

IHC

Harvested tumors were fixed in 10% neutral buffered formalin overnight, washed in 70% ethanol, and subsequently embedded in paraffin blocks. Tissue sections were stained for Ki67 using the Universal Quick kit (PK-8800, Vector Laboratories) according to the manufacturer's instructions. Antigen retrieval was performed using a decloaking chamber in 10 mmol/L citrate buffer (pH 6.0). Sections were stained with mouse anti-Ki67 (Cell Signaling Technology) overnight at 4°C. Antibody binding was revealed by addition of 3,3′-diaminobenzidine substrate

and sections were counterstained with Mayer's hematoxylin (Vector Laboratories). Ki67 staining was examined using a Nikon Eclipse microscope and quantitation of Ki67-positive nuclei from three independent sections was performed with Figi software.

Statistical analysis

Statistical differences between treatment groups in *in vitro* studies were determined using two-tailed Student *t* test. For animal studies, the differences between treatment groups were determined by the Mann–Whitney test with Bonferroni *post hoc* corrections. A P value of <0.05 was considered to be statistically significant. Error bars for all figures represent SEM and unless otherwise stated, figures are representative of at least three independent experiments.

Results

HNSCC models of acquired cetuximab resistance are dependent on alternative RTK activity

Hyperactivation of multiple RTKs has been associated with resistance to cetuximab in HNSCC (6–9, 24). To uncover a common mechanism that contributes to the upregulation of RTKs in cetuximab-resistant cells, we first generated three novel HNSCC models of acquired cetuximab resistance in the PECAPJ49, FaDu, and CAL33 cell lines. Each cell line was initially cultured with a concentration of cetuximab that resulted in approximately 50% survival. Over a period of 3–6 months, cetuximab-treated clones were continually cultured with increasing doses of cetuximab every 2–3 weeks until they displayed very little to no sensitivity to cetuximab treatment (Supplementary Fig. S1). Cetuximab-resistant (CTXR) clones were derived from each cell line and their response to cetuximab was compared with their respective parental cells in both short-term (96 hours; Fig. 1A and B; Supplementary Fig. S2A) and long-term (21 days; Supplementary Fig. S2B and S2C) assays.

Next, a phospho-RTK array was used to determine whether alternative RTK activation could be a potential mechanism of resistance to cetuximab in these models. Indeed, we observed activation of several RTKs in all CTXR clones tested. Distinct RTK activation landscapes were observed in each of the three CTXR cell lines, suggesting heterogeneity across HNSCC cell line models. For example, the PECAPJ49 CTXR clones (#1 and #4) displayed elevated levels of phosphorylated AXL and RYK compared with the PECAPJ49 parental line (Fig. 1C), while FaDu CTXR clones (#2 and #3) exhibited increased expression of AXL, MET (CTXR#2), and RYK compared with the FaDu parental line (Fig. 1D). The CAL33 CTXR clones also had unique RTK signatures characterized by increased activation of HER3, MET, and ROR2 (Supplementary Fig. S2D). Interestingly, while FaDu CTXR#2 displayed elevated MET activation, the PECAPJ49 CTXR clones exhibited decreased MET activity, further illustrating the complexity of RTK activation in cetuximab-resistant models. In addition to examining the phosphorylation status of these RTKs, we also observed that AXL protein and mRNA levels were increased in both PECAPJ49 and FaDu cetuximab-resistant clones compared with their parental counterparts (Fig. 1E and F). Increased MET protein levels were also confirmed in the FaDu cetuximab-resistant clones (Fig. 1E). In addition, increased phospho-AXL and phospho-MET levels were observed in PECAPJ49 and FaDu CTXR clones, respectively. Phosphorylated AXL was not detected by immunoblotting in the FaDu parental and CTXR clones. These findings are consistent with previous reports of cetuximab resistance, indicating that acquired resistance is associated with upregulation of multiple RTKs (6–8, 24).

BRD4 is upregulated and is important for survival in HNSCC models of acquired cetuximab resistance

On the basis of work in other malignancies (12, 13), we hypothesized that RTK upregulation in response to cetuximab is driven by the activity of the epigenetic molecule BRD4. To test this hypothesis, we evaluated the expression level and functionality of BRD4 in CTXR HNSCC models. BRD4 has been described to exist in three isoforms, a long isoform (~200 kDa) and two shorter isoforms (~115 and ~100 kDa; ref. 25). Using an antibody that detects all three isoforms of BRD4, we observed increased expression of one or both shorter isoforms of BRD4 in the PECAPJ49 and FaDu CTXR clones compared with their parental counterparts (Supplementary Fig. S3A). The specificity of the BRD4 antibody used in this assay was confirmed by treating FaDu parental and CTXR clones with MZ1, an agent that targets and degrades BRD4 (Supplementary Fig. S3B; ref. 26). To better quantitate the cumulative expression of all BRD4 isoforms, we performed intracellular flow cytometry for BRD4 in both CTXR cell line models. By flow cytometry, PECAPJ49 and FaDu parental cells displayed different basal levels of BRD4 as seen with the immunoblot. Furthermore, we observed increased and differential BRD4 expression in the CTXR clones for both PECAPJ49 and FaDu models (Fig. 2A and B). Specific expression of BRD4 by flow cytometry was also confirmed using MZ1 (Supplementary Fig. S3C and S3D).

To determine the role of BRD4 in mediating RTK expression in the setting of cetuximab resistance, we employed a genetic silencing approach using siRNAs specific to BRD4. PECAPJ49 parental and cetuximab-resistant clones were transfected with two different BRD4 siRNA oligonucleotides or a scrambled control. Each population was simultaneously treated with cetuximab. First, we confirmed the efficacy of cetuximab treatment by assessing the membrane expression of EGFR in both PECAPJ49 Parental and CTXR#4 cells treated with and without 100 nmol/L cetuximab. While we observed decreased membranous EGFR expression in CTXR#4 compared with parental cells, 100 nmol/L cetuximab significantly downmodulated EGFR expression in both cell lines (Supplementary Fig. S4). Next, we assessed viability 96 hours posttransfection with BRD4 siRNA ± cetuximab to determine whether BRD4 depletion can resensitize the resistant models to cetuximab. Both parental and cetuximab-resistant clones demonstrated increased sensitivity to BRD4 depletion (Fig. 2C). More importantly, both BRD4 siRNAs significantly resensitized the cetuximab-resistant clones to cetuximab.

In addition to BRD4 knockdown, we also found that the AXL expression in CTXR#4 was downmodulated by BRD4 siRNA to a greater degree than that observed in the parental cells (Fig. 2D). BRD4 is known to be a strong activator of *MYC* expression; therefore, as a control, we performed an immunoblot for p21 (*CDKN1A*), which is known to be strongly repressed by MYC (17). Indeed, p21 was upregulated upon BRD4 knockdown.

To further assess the expression and functionality of BRD4 in the acquired cetuximab-resistant models, we assessed the ability of BRD4 to bind to an RTK promoter. Because AXL expression has been reported to correlate with poor prognosis in patients with HNSCC and was upregulated in both PECAPJ49 and FaDu CTXR

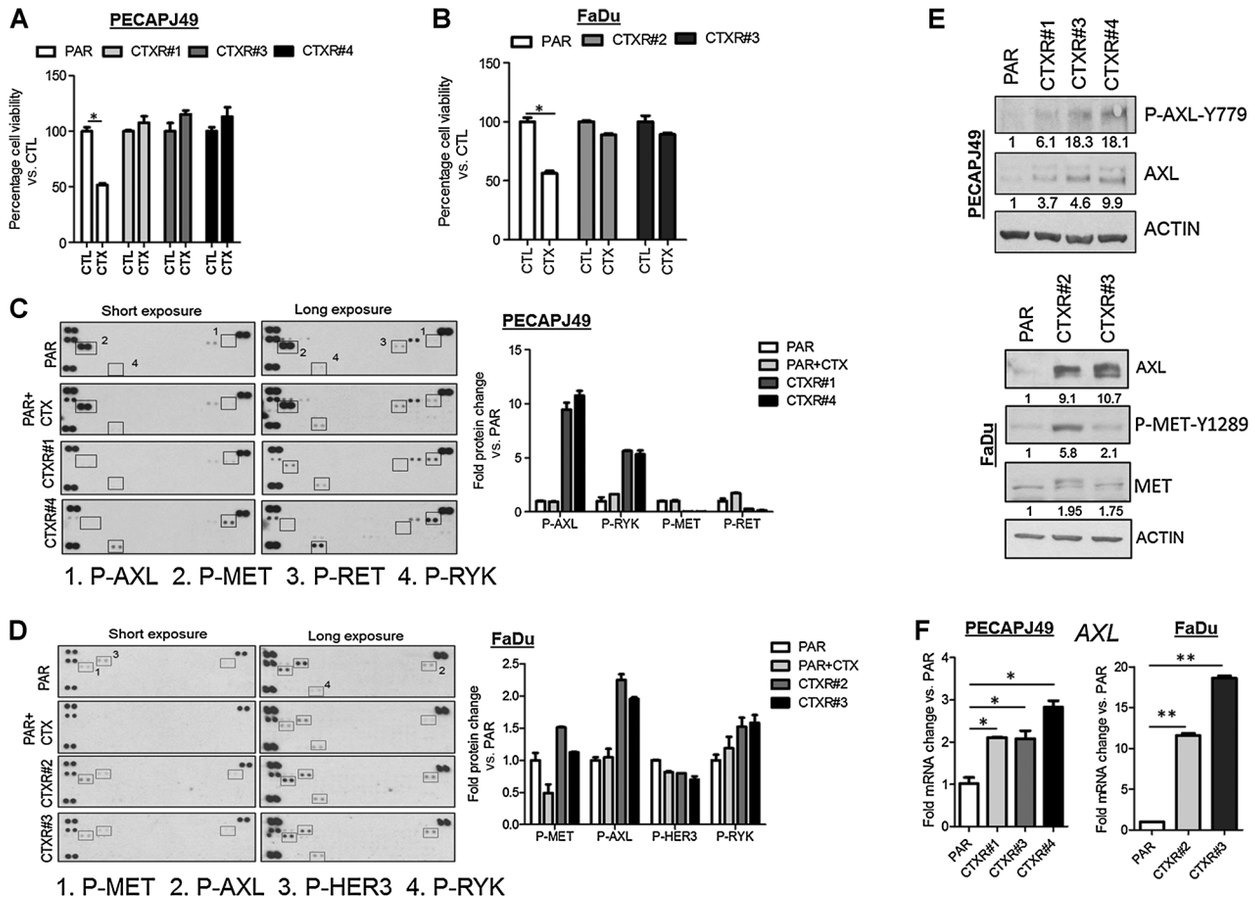

Figure 1.

Acquired cetuximab-resistant HNSCC models display heterogeneous expression of alternative RTKs. PECAPJ49 (**A**) and FaDu parental (PAR; **B**) and CTXR cell lines were treated with 100 nmol/L cetuximab (CTX) for 96 hours. Cell viability was determined by a crystal violet viability assay ($n = 4$; *, $P < 0.002$). A phospho-RTK antibody array was used to assess phosphorylated levels of various RTKs in PECAPJ49 (PAR, PAR+CTX, CTXR#1, CTXR#4; **C**) and FaDu (PAR, PAR+CTX, CTXR#2, CTXR#3) lysates ($n = 1$; **D**). Phosphorylated proteins that were altered in the CTXR clones compared with the parental line are indicated on the right. The densitometric ratio of duplicate spots for activated RTKs to the loading controls on the RTK array was calculated using Image J software. The ratios were compared with the PAR group and are represented below. **E,** Immunoblot analysis of PECAPJ49 and FaDu parental and CTXR cells for P-AXL, AXL P-MET, and MET expression was performed. Densitometry for each protein compared with actin and normalized to the parental expression is indicated below each band and is representative of three independent immunoblots. **F,** AXL mRNA expression was determined in PECAPJ49 and FaDu parental and CTXRs by RT-PCR. Fold change in AXL mRNA in CTXRs was compared with their parental counterparts ($n = 3$; *, $P = 0.01$; **, $P < 0.001$). Figure is representative of three independent experiments. Error bars, SEM.

models, we chose to examine AXL promoter status (27). We performed subcellular fractionations and a pull-down experiment using a biotinylated oligonucleotide encoding a region upstream of the AXL transcription start site to test whether nuclear BRD4 is capable of binding the AXL promoter. Increased association of BRD4 and P-CDK9 (component of p-TEFb) with the AXL promoter in PECAPJ49 CTXR#4 compared with the parental line was observed (Fig. 2E). Interestingly, we detected binding of the two BRD4 bands (~120 and ~100 kDa) in CTXR#4 compared with its parental line. It has been reported that the ~100 kDa band observed with this BRD4 antibody represents the shortest isoform of BRD4 (28). In the same publication, the band observed at ~150 kDa represented a nonspecific band (ns). This short isoform of BRD4 has been reported to mediate epithelial-to-mesenchymal transition and a stem cell–like phenotype, which is associated with drug resistance (29). Together, these approaches show that acquisition of cetuximab resistance is associated with enriched BRD4 expression and its recruitment to promoter regions of alternative RTKs and that BRD4 targeting resensitizes cetuximab-resistant cells to cetuximab.

Pharmacologic inhibition of BET family members counteracts acquired resistance *in vitro*

Following our observations with BRD4 siRNA, we investigated the sensitivity of cetuximab-resistant HNSCC models to pharmacologic inhibition of BRD4 activity. We treated the PECAPJ49 and FaDu models of acquired cetuximab resistance with the well-characterized BET inhibitor, JQ1. JQ1 binds preferentially to the bromodomains of BRD4 compared with BRD2 and BRD3 and prevents BRD4 from binding to acetylated lysines and driving transcription (17). Similar to genetic ablation of BRD4 expression, pharmacologic BET inhibition by JQ1

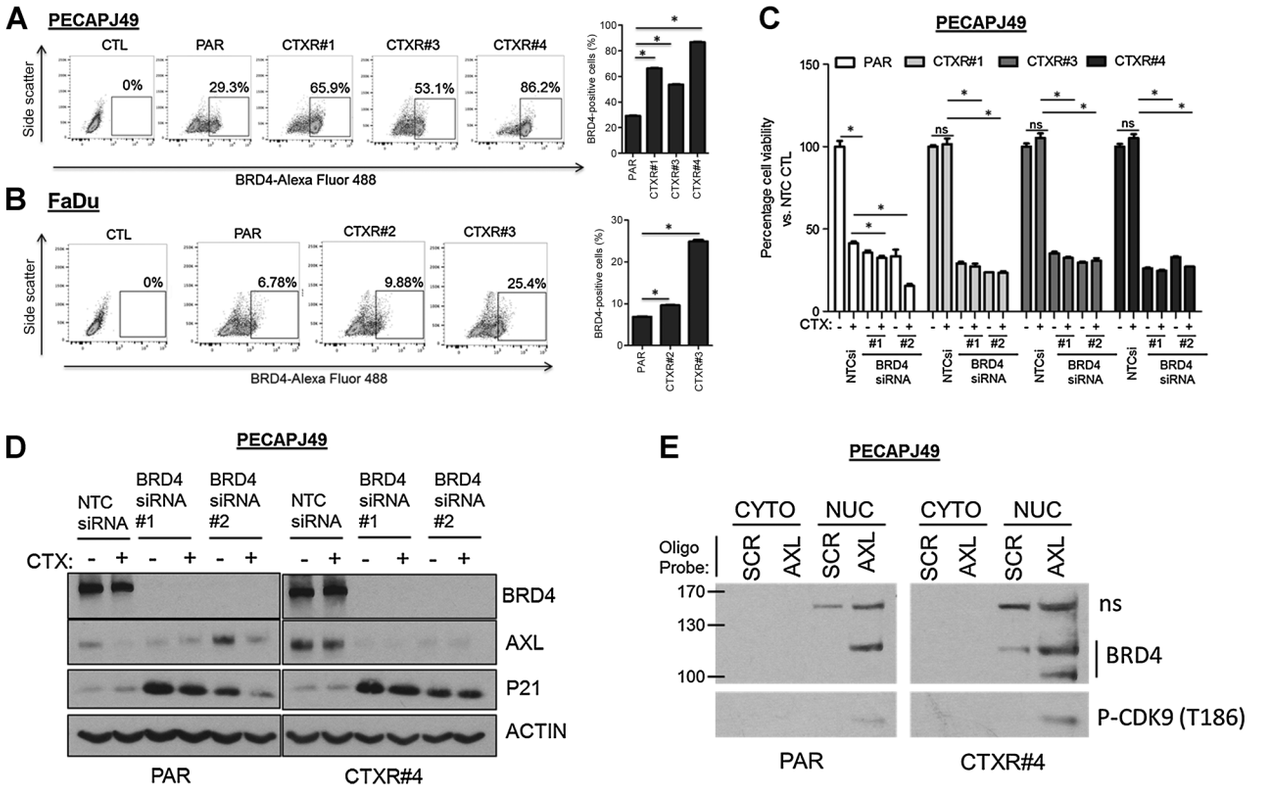

Figure 2.

Acquired cetuximab-resistant models display enriched BRD4 expression and activity. Intracellular flow cytometry for BRD4 as described in Materials and Methods was assessed in PECAPJ49 (**A**) and FaDu parental and CTXR cell line models (**B**). Rabbit Alexa-Fluor 488 secondary antibody alone (CTL) was used to set the BRD4-positive gate. Side scatter was plotted against Alexa Fluor 488 to determine the percentage of BRD4-positive cells ($n = 3$; *, $P < 0.02$). Data are representative of three independent experiments. **C,** PECAPJ49 parental and CTXRs were transfected with nontargeting control (NTC) and two BRD4 siRNA (#1, #2) oligonucleotides ± 100 nmol/L cetuximab for 96 hours. Cells were stained with crystal violet and relative cell viability was quantified ($n = 4$; *, $P < 0.02$). Figure is representative of three independent experiments. **D,** Lysates from PECAPJ49 parental and CTXR#4 cells treated with BRD4 siRNA ± 100 nmol/L cetuximab were resolved by SDS-PAGE for AXL, BRD4, and P21. β-Actin (ACTIN) was used as loading control. This figure is representative of three independent experiments. **E,** Cytoplasmic (CYTO) and nuclear (NUC) extracts of PECAPJ49 PAR and CTXR#4 cells were incubated with biotinylated scrambled (SCR) or AXL promoter region oligonucleotides. Biotinylated immunoprecipitates were resolved by SDS-PAGE and probed for BRD4 and P-CDK9 Thr186 expression (ns, nonspecific). Figure is representative of three independent experiments. Error bars, SEM.

significantly resensitized both PECAPJ49 and FaDu CTXR clones to cetuximab (Fig. 3A and B). In addition to JQ1, we also tested the efficacy of another BET inhibitor, I-BET-762 (30), at abrogating the cetuximab-resistant phenotype. Similar to JQ1, I-BET-762 resensitized parental and cetuximab-resistant clones to cetuximab treatment (Fig. 3C). We also saw similar efficacy of combined cetuximab and JQ1 treatment in a model of acquired cetuximab resistance derived from the H226 lung squamous cell carcinoma cell line, indicating that this combination therapy may be efficacious in other malignancies (Supplementary Fig. S5A and S5B).

To determine the effect of BET inhibition on RTK expression, we observed that JQ1 treatment abrogated AXL expression in both PECAPJ49 CTXR#3 and CTXR#4 clones (Fig. 3D). Interestingly, we observed that JQ1 treatment alone in the parental line augmented AXL expression compared with control-treated cells. Densitometric analysis of AXL levels indicates that JQ1 decreased AXL in both CTXR clones more so in CTXR#4 than CTXR#3. In addition to the HNSCC model, the combination of cetuximab and JQ1 potently diminished the expression of AXL in the cetuximab-resistant lung cancer clones HC4 and HC8 (Supplementary Fig. S5C).

To determine the effect of BET inhibition on BRD4 function in the PECAPJ49 CTXR model, we performed a chromatin immunoprecipitation (ChIP) assay and observed increased recruitment of BRD4 to the AXL promoter in PECAPJ49 CTXR#4 compared with the parental line (Fig. 3E). Moreover, the occupancy of BRD4 on the AXL promoter was decreased by the bromodomain inhibitor JQ1 in CTXR#4 but not in the parental line.

To address the durability of the response to combined cetuximab and JQ1 treatment, we employed a longer-term *in vitro* growth assay. The cetuximab-sensitive HNSCC cell line, CAL33, was seeded at a low density and subsequently treated with cetuximab or cetuximab+JQ1. After 21 days, the drug was removed and the cells were cultured for an additional 15 days. Cetuximab treatment and cetuximab + JQ1 robustly decreased cellular outgrowth (Fig. 3F). However, upon removal of drugs, cetuximab-treated cells displayed rapid outgrowth, while cells previously treated with the combination of cetuximab +JQ1 only showed marginal outgrowth.

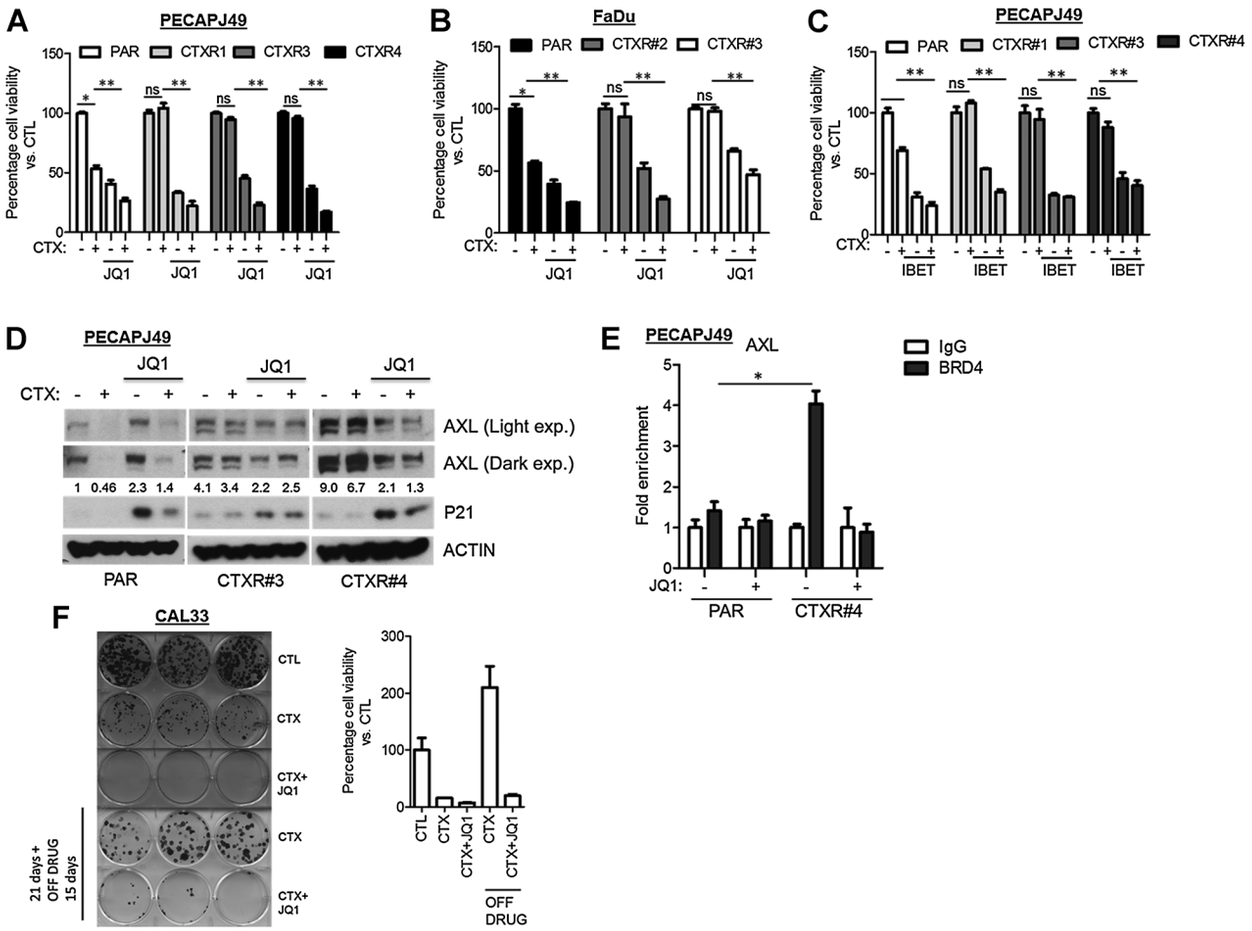

Figure 3.

Bromodomain inhibition sensitizes acquired cetuximab-resistant models to cetuximab. **A** and **B,** PECAPJ49 (**A**), FaDu (**B**), and CTXR cells were treated with 100 nmol/L cetuximab (CTX) ± 300 nmol/L JQ1 for 72 hours. Cell viability was assessed by crystal violet assay ($n = 3$; *, $P < 0.05$; **, $P < 0.01$; ns, not significant). **C,** PECAPJ49 parental and cetuximab-resistant clones were treated with 100 nmol/L cetuximab ± 800 nmol/L I-BET-762(IBET) for 72 hours. Cells were stained with crystal violet and quantified as described in Materials and Methods ($n = 3$; *, $P < 0.02$). Figures are representative of three independent experiments. **D,** PECAPJ49 parental and CTXR#3, #4 lines were treated with cetuximab ± JQ1 for 72 hours. Lysates were resolved and assessed for AXL (dark and light exposures), P21, and ACTIN. Densitometric analysis of AXL expression normalized to PAR CTL from three independent immunoblots is indicated below AXL bands. **E,** ChIP-qPCR analysis for BRD4 occupancy on the AXL promoter of PECAPJ49 PAR and CTXR#4 cells treated with or without 300 nmol/L JQ1 was performed. Fold enrichment was determined by the $\Delta\Delta C_t$ method and then the BRD4 occupancy was compared with IgG occupancy and presented as a fold enrichment score ($n = 3$; *, $P = 0.003$). Figure is representative of two independent experiments. **F,** CAL33 cells were seeded at 250 cells/well in 6-well dishes and treated with control (CTL), cetuximab, or cetuximab+JQ1 every 3 days for 21 days. After 21 days, drug treatment was withdrawn for 15 days, and cells were stained with crystal violet to assess viability ($n = 3$). Figure is representative of two independent experiments. Error bars, SEM.

Together, the results in this section suggest that bromodomain targeting can effectively overcome cetuximab resistance and suppress the expression of alternative RTKs known to drive cancers with cetuximab-resistant phenotypes.

BET blockade abrogates RTK expression in cetuximab-resistant HNSCC models

To determine whether this therapeutic strategy can be applied to intrinsically cetuximab-resistant models, we treated intrinsically cetuximab-resistant HNSCC cell lines with the combination of cetuximab and JQ1. First, we sought to determine whether there was an association between BRD4 expression and intrinsic cetuximab response in HNSCC cell lines. We assessed the expression levels of BRD4 across a panel of intrinsically cetuximab-sensitive and -resistant models by both immunoblotting and flow cytometry (Supplementary Fig. S6A and S6B). With the exception of HSC6 and SCC47, there was no clear correlation between the basal expression of BRD4 and cetuximab resistance across the panel of cell lines tested. Next, we treated the intrinsically resistant cells with cetuximab or the combination of cetuximab and JQ1 (Fig. 4A). All of the intrinsically resistant cell lines were significantly sensitized to cetuximab upon cotreatment with JQ1. To determine whether sensitization of intrinsically resistant cells to cetuximab by JQ1 was due to RTK downregulation, we first performed a phosphorylated RTK array with the intrinsically cetuximab-resistant cell line CAL27 treated with cetuximab or the combination of cetuximab and JQ1 for 72 hours (Fig. 4B). While cetuximab

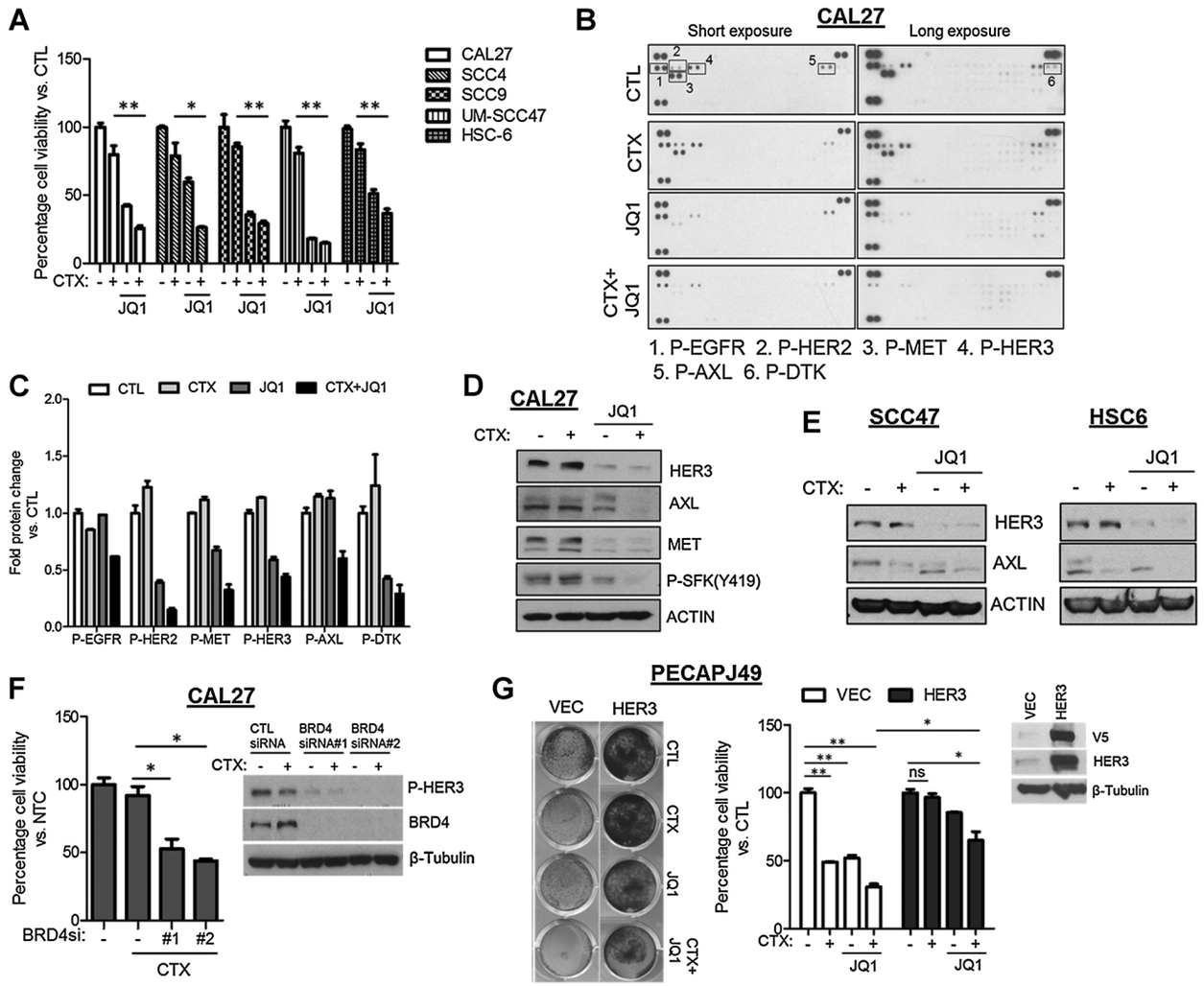

Figure 4.

Bromodomain inhibition abrogates RTK expression in intrinsically cetuximab-resistant models. **A,** Intrinsically cetuximab (CTX)-resistant cell lines were treated with 100 nmol/L cetuximab and 300 nmol/L JQ1 for 72 hours. Cell viability was assessed by crystal violet assay ($n = 3$; *, $P < 0.04$; **, $P < 0.01$). Figure is representative of three independent experiments. **B,** CAL27 cells were treated with control (CTL), 100 nmol/L cetuximab, 300 nmol/L JQ1, and cetuximab+JQ1 for 72 hours. Lysates were procured, and activated RTK expression was assessed using a phospho-RTK array ($n = 1$). **C,** The densitometric ratio of duplicate spots for activated RTKs to the loading controls on the RTK array was calculated using Image J software. The ratios were compared with the control group and are represented. **D,** CAL27 lysates were also resolved by SDS-PAGE for expression of total HER3, MET, AXL, and phospho-SFK. Figure is representative of three independent immunoblots. **E,** SCC47 and HSC6 cells were treated with 100 nmol/L cetuximab ± 300 nmol/L JQ1 for 72 hours. Lysates were resolved and assessed for HER3, AXL, and ACTIN expression. Figures are representative of two independent immunoblots. **F,** Intrinsically cetuximab-resistant HNSCC cell line CAL27 was treated with control (CTL) siRNA, CTL + cetuximab, cetuximab + BRD4si#1, and cetuximab + BRD4si#2 for 96 hours. Cell viability was assessed by crystal violet assay ($n = 3$; *, $P < 0.01$). Figure is representative of three independent experiments. CAL27 cells treated with CTL siRNA or BRD4 siRNA ± cetuximab for 96 hours were interrogated for phosphorylated HER3, BRD4 expression, and β-tubulin, which was used as the loading control. Figure is representative of three independent experiments. **G,** PECAPJ49 vector (VEC) and HER3-expressing cells were treated with vehicle, 100 nmol/L cetuximab, 300 nmol/L JQ1, or cetuximab ± JQ1 for 72 hours. Cell viability was assessed by crystal violet assay. Images of representative wells stained with crystal violet are illustrated ($n = 3$; *, $P < 0.05$; **, $P < 0.02$). Figure is representative of three independent experiments. Immunoblot analysis of vector and HER3-expressing cells for V5, HER3, and β-tubulin was performed and is illustrated on the right. Figure is representative of two independent immunoblots. Error bars, SEM.

modestly increased RTK activation, the combination treatment markedly decreased the activation of several RTKs, including HER2, HER3, MET, and DTK as observed by densitometric analysis (Fig. 4C). We validated that the decreased phosphorylated RTK levels in CAL27 were due to lowered total RTK expression by immunoblot and also found that this was associated with a decrease in phosphorylated Src Family Kinases (SFK), which are downstream effectors of multiple RTKs (Fig. 4D). HER3 and AXL expression was also decreased by this combination in SCC47 and HSC6, which are intrinsically cetuximab resistant and have augmented levels of BRD4 (Fig. 4E). We also validated the effects of BRD4 inhibition in

the intrinsically cetuximab-resistant line CAL27 using genetic knockdown. BRD4 knockdown resulted in a significant increase in sensitivity to cetuximab compared with cetuximab treatment alone (Fig. 4F). Immunoblots revealed downregulation of phosphorylated HER3 upon BRD4 knockdown in CAL27 cells with and without cetuximab (Fig. 4F). These results demonstrate that BRD4 targeting sensitizes resistant cells to cetuximab and can regulate RTK expression in the cetuximab-resistant HNSCC models exposed to cetuximab. In addition, these results indicate that BRD4 expression is not a clear predictor of intrinsic cetuximab resistance in HNSCC cell lines.

RTK overexpression mediates resistance to cetuximab and BET inhibition

We next sought to determine whether the sensitivity of cetuximab-resistant cells to BET inhibition was in part due to abrogation of RTK expression. We stably introduced either a vector control or HER3 overexpression vector in the cetuximab-sensitive cell line PECAPJ49. Both vector and HER3-expressing cells were treated with cetuximab or the combination of cetuximab and JQ1 for 72 hours. As expected, the vector control cells were sensitive to all treatment modalities (Fig. 4G). Interestingly, HER3 overexpression was capable of mitigating all cetuximab sensitivity in this cell line. While HER3-overexpressing cells were still sensitive to the combination of cetuximab and JQ1, these cells were significantly less sensitive than the vector control cells. Immunoblotting confirmed exogenous expression of HER3-V5 expression in the HER3-expressing cells compared with the vector-expressing cell line. Taken together, these data suggest that RTK overexpression can mediate cetuximab resistance and that BET inhibition overcomes cetuximab resistance in part by diminishing RTK expression.

BET blockade prevents acquisition of cetuximab resistance in HNSCC PDX models

To translate our *in vitro* findings into preclinical models, we investigated the effect of BET blockade on cetuximab resistance using two HNSCC PDX models (PDX-6282 and PDX-7157). While basal expression of BRD4 by immunoblotting was difficult to detect in these PDX models, PDX-7157 had very low expression of one of the short isoforms of BRD4 (Supplementary Fig. S6C). We transplanted each PDX into mice and allowed the tumors to grow to approximately 100 mm^3. Mice were then treated with vehicle, cetuximab, JQ1, or the combination of JQ1 plus cetuximab. Both PDX models demonstrated initial sensitivity to cetuximab but eventually developed a recurrent growth phenotype (Fig. 5A and B). Neither PDX was significantly sensitive to JQ1 alone, possibly due to the low basal levels of BRD4. Strikingly, the combination of cetuximab and JQ1 delayed tumor outgrowth in both PDX models (Fig. 5A and B; CTX vs. CTX+JQ1, PDX6282: $P = 0.04$; PDX7157: $P = 0.003$). To determine the heterogeneity of activated RTKs altered upon treatment in these PDX models, we performed a phospho-RTK array using lysates procured from both PDXs treated in all four treatment groups. Interestingly, PDX-6282 tumors that demonstrated outgrowth following cetuximab treatment exhibited increased levels of activated HER2, HER3, Tie2, and ROR2 among others (Fig. 5C; Supplementary Fig. S7A). The PDX-7157 tumors that displayed outgrowth following cetuximab showed upregulation of activated RYK, INSR, DDR1, and ROR2 (Fig. 5D; Supplementary Fig. S7B). The combination of cetuximab and JQ1 abrogated activated levels of all these RTKs in both models (Fig. 5C and D). On the basis of the results of the RTK array, we interrogated total RTK expression in PDX-6282 by immunoblotting for HER2, HER3, and ROR2. With the exception of tumor #4, each RTK was robustly abrogated in the combined cetuximab and JQ1-treated tumors compared with all other treatment groups (Fig. 5E). In addition, the combination of cetuximab and JQ1 robustly decreased downstream signaling components of RTKs including phospho-SFKs, phospho-ERK1/2, and Myc expression (Fig. 5E). Of note, we also observed downmodulation of phosphorylated ERK1/2 in the cetuximab-treated groups, which demonstrated the efficacy of cetuximab in this experiment. In line with the hypothesis that cetuximab resistance is associated with heterogenous RTK activation from model to model, P-AXL was not upregulated in the RTK array and total expression was difficult to interpret by immunoblotting (Supplementary Fig. S7C and S7D). In addition, based on the RTK array and previous reports, P-EGFR and EGFR levels were expressed in the tumors that outgrew with cetuximab treatment (Fig. 5C; Supplementary Fig. S7D; refs. 8, 31). IHC analysis of the PDXs treated with cetuximab expressed high Ki67 levels compared with tumor sections from the JQ1 and combination groups (Supplementary Fig. S7E). Because of the high efficacy of combined cetuximab and JQ1 treatment in these models, we were only able to evaluate three independent sections from one of the tumors in the CTX+JQ1 treatment group. These results suggest that JQ1 can prevent the acquisition of cetuximab resistance in part by abrogation of RTK expression in preclinical models of HNSCC.

RTK and BRD4 gene expression in clinical HNSCC cohorts

To further assess the translational relevance of the findings in this article, we interrogated publicly available microarray data from a cohort of 40 patients with HNSCC treated with platinum and cetuximab therapy (NCBI GEO GSE65021; ref. 32). From this cohort, 14 patients displayed long progression-free survival (PFS > 12 months) and 26 patients displayed short PFS (PFS < 5.6 months). From the patient samples that were graded as moderately/poorly differentiated and procured from the oral cavity and larynx ($n = 25$), we observed that *AXL* and *ROR2* expression was significantly higher in short PFS patients compared with the long PFS patients (Fig. 5F). Five of the 8 moderately to poorly differentiated tumors from the oropharynx region were human papillomavirus (HPV)-positive and excluded from the analysis. In addition, other RTKs that were activated in the cetuximab-treated PDXs such as Tie-2 (*TEK*) and INSR as seen in Fig. 5C and D, trended toward upregulation in short PFS patients compared with long PFS patients although they lacked statistical significance (Supplementary Fig. S8). Interestingly, we observed no difference in *BRD4* gene expression between the short and long PFS patient samples (Fig. 5G). However, analysis of The Cancer Genome Atlas (TCGA) and GTEx databases (33), revealed that BRD4 is significantly higher in HNSCC tumor tissue compared with normal oral/esophageal tissue (Fig. 5H). Cumulatively, these observations indicate that elevated RTK expression is associated with poor prognosis in patients with recurrent-metastatic HNSCC placed on cetuximab treatment regimens. Furthermore, the high expression of BRD4 in HNSCC tumors relative to normal tissue makes it an

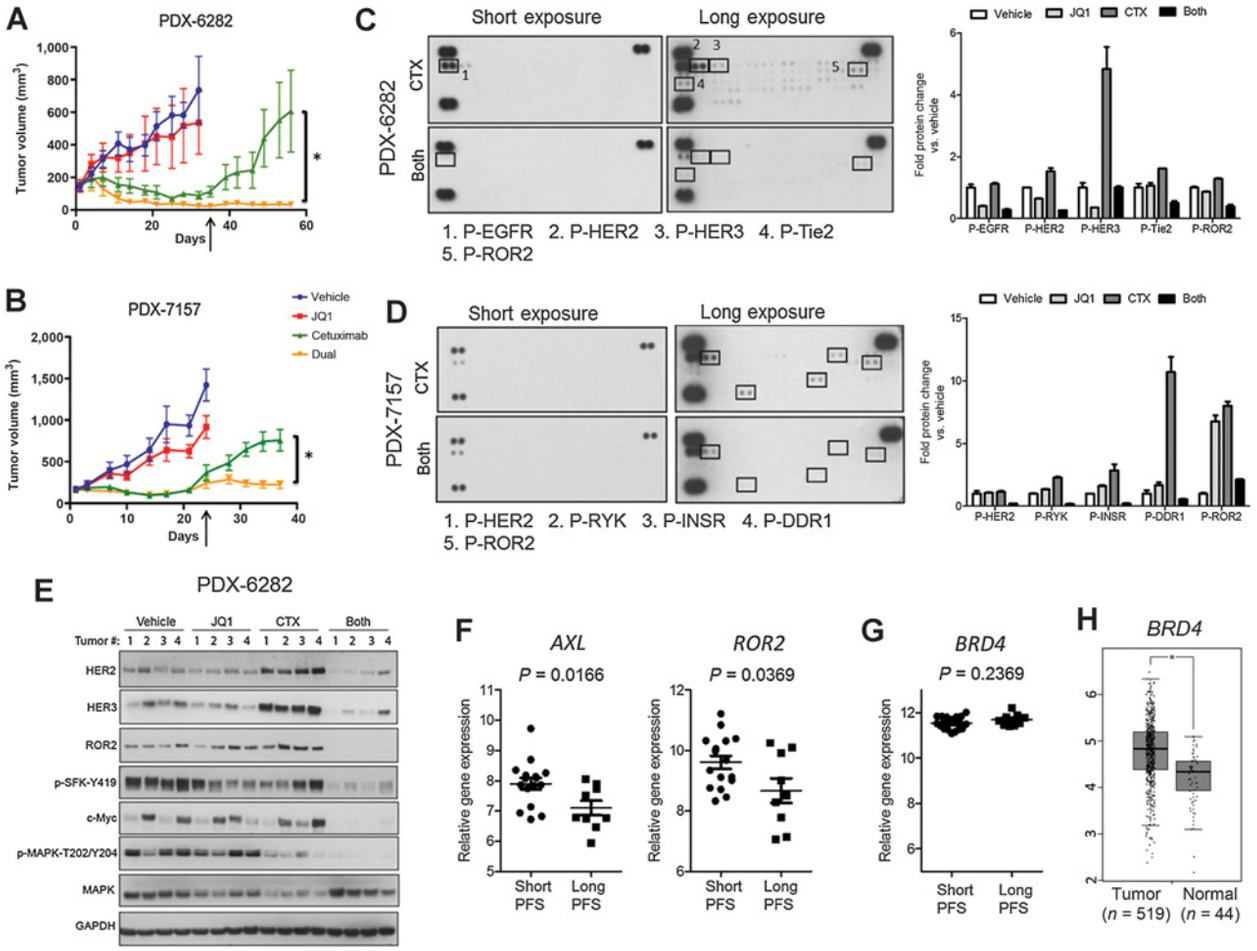

Figure 5.

JQ1 treatment prevents acquisition of cetuximab resistance in HNSCC PDX models. **A** and **B,** Two HNSCC PDX models (6282 and 7157) were implanted into NOD/SCIDγ mice and separated into four treatment groups ($n = 6$/group): i, vehicle; ii, cetuximab (CTX; 20 mg/kg via i.p); iii, JQ1 (50 mg/kg via i.p, 5qd); iv, cetuximab + JQ1. Mice were treated with two doses of cetuximab on days 1 and 5. Tumors were measured twice weekly and plotted ($P < 0.01$; JQ1 vs. CTX+JQ1, $P < 0.001$; vehicle vs. CTX, $P = 0.04$ (PDX6282), $P = 0.003$ (PDX7157); CTX vs. CTX+JQ1). Arrows, point at which tumors began to regrow. **C** and **D,** Phospho-RTK arrays using lysates harvested from PDXs 6282 (**C**) and 7157 (**D**) at the last time point were performed. Phosphorylated RTKs that were augmented in the PDXs that acquired cetuximab resistance and abrogated with combination of JQ1 are indicated ($n = 1$). The densitometric ratio of duplicate spots for activated RTKs and the loading controls on the RTK arrays was calculated using Image J software. The ratios were compared with the vehicle-treated group and are represented. **E,** Lysates from four PDX6282 tumors in each treatment group were resolved by SDS-PAGE for HER2, HER3, ROR2, P-SFK, P-MAPK, total MAPK, and GAPDH (loading control). This figure is representative of two independent immunoblots. *AXL, ROR2* (**F**), and *BRD4* (**G**) gene expression data from WG-DASL (whole-genome cDNA-mediated annealing, selection, extension, and ligation) microarray data of 40 patients with HNSCC treated with first-line platinum and cetuximab therapy were analyzed (NCBI GEO GSE65021; ref. 32). The moderately and poorly differentiated tumors obtained from the oral cavity and larynx were analyzed ($n = 25$). *y*-axis, $\log_2$-transformed values of the processed gene expression data (*AXL*, $P = 0.0166$; *ROR2*, $P = 0.0369$; BRD4, $P = 0.2369$). **H,** BRD4 expression from TCGA HNSCC tumor and normal tissues was assessed using the GEPIA web server (33). The custom *P* value cutoff was 0.01. *y*-axis, log-transformed relative gene expression.

attractive therapeutic target to improve the prognosis of patients with moderately and poorly differentiated HNSCC treated with cetuximab.

Discussion

The expression and activity of different RTKs have been shown to mediate resistance to the FDA-approved EGFR inhibitor cetuximab, but the simultaneous targeting of multiple RTKs is not likely to yield positive clinical results due to the availability of alternative resistance mechanisms and anticipated toxicity (6–9). In this article, we sought to evaluate a single molecular target that can enhance the antitumor effects of cetuximab by diminishing activation/expression of alternative RTKs. We hypothesized that targeting the bromodomain and extra terminal protein BRD4 could abrogate RTK expression and overcome cetuximab resistance. We observed that cell line models of acquired cetuximab resistance expressed increased RTKs and were enriched for BRD4 expression and functionality. Both genetic and pharmacologic targeting of BRD4-sensitized cell line models to cetuximab and robustly decreased RTK expression. In addition, blockade of BRD4 with the

bromodomain inhibitor JQ1 delayed the acquisition of cetuximab resistance in PDX models of HNSCC. Both PDXs displayed a heterogeneous upregulation of activated RTKs, which were all abrogated with JQ1 treatment. Finally, we observed increased RTK expression in patients with cetuximab-treated HNSCC with short PFS and elevated BRD4 levels in HNSCC tumors compared with normal oral tissue. These findings suggest that blockade of BRD4 is a promising therapeutic strategy to enhance the efficacy of cetuximab in patients with HNSCC by preventing oncogenic signaling driven by alternative RTKs.

Previous studies have implicated various RTKs, such as MET, AXL, IGF1R, and HER3, in mediating cetuximab resistance in various cancer models, including HNSCC (6–8, 34, 35). For example, a report on cetuximab-resistant colon cancer identified increased expression of MET, AXL, and IGF1R in a xenograft model (10). They further showed that suppression of long-term tumor growth following EGFR inhibition was only achieved when combined administration of inhibitors targeting all three of these RTKs was performed. Most alternative approaches to overcome signaling mediated by multiple RTKs are centered on targeting common downstream effectors such as Akt, ERK, or Src family kinases (SFK). Only modest clinical efficacy was reported in a phase II trial of cetuximab combined with the SFK inhibitor dasatinib in patients with HNSCC, which may be due to the activation of Src kinase–independent signaling pathways (36). Moreover, single-agent administration of another SFK inhibitor saracatinib displayed a lack of efficacy in a trial of metastatic and recurrent HNSCC (37). Other groups have found that targeting the AKT/mTOR pathway can overcome cetuximab resistance in HNSCC preclinical models harboring *PIK3CA* and *RAS* mutations, suggesting that the identification of predictive biomarkers may enhance our ability to deliver the most promising combination strategies to the right patient population (38, 39). In this study, we sought to elucidate a common target upstream of multiple RTKs to be inhibited in combination with cetuximab to increase therapeutic durability. Our findings suggest that targeting BRD4 may overcome cetuximab resistance in multiple cetuximab-resistant HNSCC models independent of genetic predisposition. For example, the cell lines used in this article display broad genetic heterogeneity; PECAPJ49 cells harbor a NOTCH1 mutation,; FaDu cells are SMAD4 mutant; CAL27 has APC and CASP8 mutations; and HSC6 cells are MAPK1 mutant (40).

With the heterogenous upregulation of RTKs observed in our three models of cetuximab resistance, we noticed that while FaDu cetuximab–resistant cells displayed increased MET activity and expression, PECAPJ49 cetuximab–resistant cells exhibited diminished MET activity. This observation indicated the possibility that chronic cetuximab treatment may result in histone acetylation and BRD4 recruitment at different enhancer and promoter regions in a context-dependent manner. A recent study by Zawistowski and colleagues showed that basal-like and claudin-low triple-negative breast cancer cells displayed a differential kinome profile in response to the MEK inhibitor trametinib. In addition, they demonstrated that isogenically similar subpopulations from a TNBC cell line upregulated different RTKs following MEK inhibition (41). These results combined with our observations further indicate the important role that chromatin regulation events play in various models of drug resistance independent of tumor classifications, and the need to develop targeting strategies to exploit their dynamic effects.

While RTKs such as HER3, MET, and AXL are well known mediators of cetuximab resistance, our analyses also identified additional RTKs that may contribute to cetuximab resistance. For example, ROR2 was identified in both cetuximab-resistant PDX models and patients with cetuximab-treated HNSCC (Fig. 5C, D, and F). ROR2 is an orphan RTK that is known to mediate β-catenin–independent Wnt signaling. Moreover, the Wnt5A–ROR2 signaling axis is a major driver of tongue SCC metastasis and is associated with poor prognosis (42). In aggressive basal-like breast cancer, BRD4 was shown to interact with acetylated Twist via bromodomain 2 to drive transcription of Wnt5A (43). Recent studies have also found increased ROR2 expression in cisplatin-resistant models of ovarian cancer, and downmodulation of ROR2 activity decreased the epithelial-to-mesenchymal (EMT) phenotype of these cisplatin-resistant cells (44). In addition, expression of the RYK receptor was increased in PECAPJ49 and FaDu cetuximab–resistant HNSCC cell lines and cetuximab-resistant PDX-7157 (Figs. 1C and D and 5C and D). Similar to ROR2, RYK functions as a coreceptor in the Wnt pathway (45). High-throughput genetic analysis of HNSCC PDXs and patient samples from the TCGA identified subsets of samples with basal and mesenchymal gene signatures (46, 47). PDXs expressing the basal gene signature displayed cetuximab sensitivity while the PDXs with the mesenchymal or EMT gene signature were cetuximab resistant (47). Furthermore, mesenchymal PDXs displayed robust expression of Wnt5A compared with the PDXs with a basal gene signature. Given the critical roles of these understudied RTKs in the drug-resistant EMT phenotype, which predicts cetuximab resistance in patients with HNSCC, and the lack of selective targeting agents against these proteins, BET inhibition may be a promising alternative approach to inhibit orphan RTKs through one unifying approach.

Both immunoblot and flow cytometric analysis of BRD4 expression in the PECAPJ49 and FaDu models of acquired cetuximab resistance indicated varying levels of BRD4 and its various short isoforms among the clones. BRD4 has been shown to exist as three isoforms (A, B, and C) with A being the long isoform with B and C being the two shorter isoforms. In the PECAPJ49 CTXR clones, we observed increased expression of isoform C while in the FaDu clones we observed increased expression of both B and C isoforms. It has been shown that the shorter isoforms of BRD4 mediated epithelial-to-mesenchymal transition (EMT) and breast cancer survival (29, 48). As discussed in the previous paragraph, the under-targeted RTKs such as ROR2 and RYK play roles in EMT and tumor invasion. Therefore, a more in-depth study into the roles of the short BRD4 isoforms in the CTXR models is warranted and being currently pursued. To understand the varying expression levels of BRD4 among the CTXR clones derived from a parental cell line and in the PDX models used, it is possible that the proteomic stability of BRD4 is differentially altered because we did not observe significant differences in BRD4 mRNA levels from the cohort of patients with cetuximab-treated HNSCC with short and long PFS (Fig. 5G). Two possible mechanisms have been proposed to regulate the stability of BRD4. Phosphorylation at Ser492 on BRD4 by casein kinase II has been shown enhance its recruitment to acetylated lysines, recruit the P-TEFB complex, and drive transcription (49, 50). Second, a report by Hu and colleagues demonstrated a role for prolyl isomerase 1 (PIN1) in mediating stability of BRD4 by physically interacting with it and preventing its ubiquitin-based

degradation (51). PIN1 was shown to interact with a phosphorylated threonine residue on BRD4 and facilitate its interaction P-TEFB. These studies indicate that interrogation of these proteins that regulate BRD4 stability in addition to factors that manipulate histone acetylation can predict patients that will benefit most from BET inhibitor therapy.

While JQ1 is widely considered a tool compound due to its short half-life, the next generation of bromodomain inhibitors is currently being evaluated in clinical trials for various solid and hematologic malignancies (52). In fact, a few studies have already identified resistance mechanisms to bromodomain inhibitors. A study in breast cancer found that JQ1-resistant cells displayed increased phosphorylated BRD4 and MYC expression, although the underlying mechanism was not determined (53). In another study, authors observed increased enhancer element occupancy by β-catenin in BET inhibitor–resistant leukemia cells (54). Finally, in a recent study with ovarian cancer, resistance to bromodomain inhibition was driven by upregulation of RTKs through a mechanism yet to be determined (55). Although we observed decreased viability with monotherapeutic BRD4 inhibition in cetuximab-sensitive cell lines *in vitro*, JQ1 treatment alone modestly altered PDX tumor growth and RTK expression (Fig. 5A, B and E). In fact, JQ1 treatment alone in the cetuximab-sensitive PECAPJ49 cell line augmented AXL expression that can promote a JQ1-resistant phenotype and corroborate the recent findings observed in JQ1-resistant ovarian cancer (55). Cumulatively, these observations may foreshadow the importance of cetuximab-induced epigenetic rewiring and combinatorial therapeutic approaches involving bromodomain inhibitors, rather than monotherapy.

Although the efficacy of JQ1 in HNSCC models have been previously described (56), we are the first group to provide evidence that targeting the chromatin reader BRD4 is a viable strategy to overcome cetuximab resistance in preclinical models of HNSCC and NSCLC. We also demonstrate that the underlying mechanism for the therapeutic potency is through the downregulation of cetuximab-induced alternative RTK expression and activity. Furthermore, we successfully applied this targeting strategy in two different PDX models, illustrating that this therapeutic combination can be effectively used to treat heterogeneous drug-resistant tumors. Future work will be performed to determine how BET inhibition influences response to standard-of-care and immune-based therapies that are approved for HNSCC treatment.

Disclosure of Potential Conflicts of Interest

No potential conflicts of interest were disclosed.

Authors' Contributions

Conception and design: B. Leonard, T.M. Brand, N.E. Bhola
Development of methodology: T.M. Brand, N.E. Bhola
Acquisition of data (provided animals, acquired and managed patients, provided facilities, etc.): B. Leonard, T.M. Brand, R.A. O'Keefe, E. Lee, Y. Zang, J.D. Kemmer, H. Li, N.E. Bhola
Analysis and interpretation of data (e.g., statistical analysis, biostatistics, computational analysis): B. Leonard, T.M. Brand, R.A. O'Keefe, Y. Zang, N.E. Bhola
Writing, review, and/or revision of the manuscript: B. Leonard, R.A. O'Keefe, J.R. Grandis, N.E. Bhola
Study supervision: N.E. Bhola

Acknowledgments

The authors would like to acknowledge James Bradner (Novartis) for providing JQ1 for *in vitro* studies performed in this article. This article was supported by the NIH NIDCR F32 Fellowship (to B. Leonard), American Cancer Society Post-Doctoral fellowship (to T.M. Brand), NIH NIDCR F31 Fellowship (to R.A. O'Keefe), American Cancer Society grant (to J.R. Grandis), and Brandon Gromada Head and Neck Foundation (to N.E. Bhola). The Gladstone Flow Cytometry Core is supported by NIH P30 AI027763.

The costs of publication of this article were defrayed in part by the payment of page charges. This article must therefore be hereby marked *advertisement* in accordance with 18 U.S.C. Section 1734 solely to indicate this fact.

Received February 14, 2018; revised April 21, 2018; accepted May 18, 2018; published first May 23, 2018.

References

1. Ferlay J, Shin HR, Bray F, Forman D, Mathers C, Parkin DM. Estimates of worldwide burden of cancer in 2008: GLOBOCAN 2008. Int J Cancer 2010;127:2893–917.
2. Bonner JA, Harari PM, Giralt J, Cohen RB, Jones CU, Sur RK, et al. Radiotherapy plus cetuximab for locoregionally advanced head and neck cancer: 5-year survival data from a phase 3 randomised trial, and relation between cetuximab-induced rash and survival. Lancet Oncol 2010;11:21–8.
3. Bardelli A, Corso S, Bertotti A, Hobor S, Valtorta E, Siravegna G, et al. Amplification of the MET receptor drives resistance to anti-EGFR therapies in colorectal cancer. Cancer Discov 2013;3:658–73.
4. Diaz LA, Williams R, Wu J, Kinde I, Hecht JR, Berlin J, et al. The molecular evolution of acquired resistance to targeted EGFR blockade in colorectal cancers. Nature 2012;486:537–40.
5. Brand TM, Iida M, Wheeler DL. Molecular mechanisms of resistance to the EGFR monoclonal antibody cetuximab. Cancer Biol Ther 2011; 11:777–92.
6. Madoz-Gúrpide J, Zazo S, Chamizo C, Casado V, Caramés C, Gavín E, et al. Activation of MET pathway predicts poor outcome to cetuximab in patients with recurrent or metastatic head and neck cancer. J Transl Med 2015;13:282.
7. Jiang N, Wang D, Hu Z, Shin HJC, Qian G, Rahman MA, et al. Combination of anti-HER3 antibody MM-121/SAR256212 and cetuximab inhibits tumor growth in preclinical models of head and neck squamous cell carcinoma. Mol Cancer Ther 2014;13: 1826–36.
8. Brand TM, Iida M, Stein AP, Corrigan KL, Braverman CM, Luthar N, et al. AXL mediates resistance to cetuximab therapy. Cancer Res 2014;74: 5152–64.
9. Wheeler DL, Huang S, Kruser TJ, Nechrebecki MM, Armstrong EA, Benavente S, et al. Mechanisms of acquired resistance to cetuximab: role of HER (ErbB) family members. Oncogene 2008;27:3944–56.
10. Hu S, Dai H, Li T, Tang Y, Fu W, Yuan Q, et al. Broad RTK-targeted therapy overcomes molecular heterogeneity-driven resistance to cetuximab via vectored immunoprophylaxis in colorectal cancer. Cancer Lett 2016;382: 32–43.
11. Samatar AA, Poulikakos PI. Targeting RAS-ERK signalling in cancer: promises and challenges. Nat Rev Drug Discov 2014;13:928–42.
12. Stuhlmiller TJ, Miller SM, Zawistowski JS, Nakamura K, Beltran AS, Duncan JS, et al. Inhibition of lapatinib-induced kinome reprogramming in ERBB2-positive breast cancer by targeting BET family bromodomains. Cell Rep 2015;11:390–404.
13. Stratikopoulos Elias E, Dendy M, Szabolcs M, Khaykin Alan J, Lefebvre C, Zhou MM, et al. Kinase and BET inhibitors together clamp inhibition of PI3K signaling and overcome resistance to therapy. Cancer Cell 2015; 27:837–51.
14. Zeng L, Zhou MM. Bromodomain: an acetyl-lysine binding domain. FEBS Lett 2002;513:124–8.

15. Yang Z, Yik JHN, Chen R, He N, Jang MK, Ozato K, et al. Recruitment of P-TEFb for stimulation of transcriptional elongation by the bromodomain protein Brd4. Mol Cell 2005;19:535–45.
16. Marshall NF, Peng J, Xie Z, Price DH. Control of RNA polymerase II elongation potential by a novel carboxyl-terminal domain kinase. J Biol Chem 1996;271:27176–83.
17. Filippakopoulos P, Qi J, Picaud S, Shen Y, Smith WB, Fedorov O, et al. Selective inhibition of BET bromodomains. Nature 2010;468:1067–73.
18. Zuber J, Shi J, Wang E, Rappaport AR, Herrmann H, Sison EA, et al. RNAi screen identifies Brd4 as a therapeutic target in acute myeloid leukaemia. Nature 2011;478:524–8.
19. Shi JB, Wu PF, Lin HS, Lin YT, Lee HW, Kao CT, et al. Synthesis and characterization of single-crystalline zinc tin oxide nanowires. Nanoscale Res Lett 2014;9:210.
20. Brand TM, Hartmann S, Bhola NE, Peyser ND, Li H, Zeng Y, et al. Human papillomavirus regulates HER3 expression in head and neck cancer: implications for targeted HER3 therapy in HPV^{+} patients. Clin Cancer Res 2017;23:3072–83.
21. Suzuki K, Bose P, Leong-Quong RY, Fujita DJ, Riabowol K. REAP: a two minute cell fractionation method. BMC Res Notes 2010;3:294.
22. Wu KK. Analysis of protein-DNA binding by streptavidin-agarose pull-down. In: Bina M, editor. Gene mapping, discovery, and expression: methods and protocols. Totowa, NJ: Humana Press; 2006. p. 281–90.
23. Li H, Wheeler S, Park Y, Ju Z, Thomas SM, Fichera M, et al. Proteomic characterization of head and neck cancer patient–derived xenografts. Mol Cancer Res 2016;14:278–86.
24. Jun HJ, Acquaviva J, Chi D, Lessard J, Zhu H, Woolfenden S, et al. Acquired MET expression confers resistance to EGFR inhibition in a mouse model of glioblastoma multiforme. Oncogene 2012;31:3039–50.
25. Floyd SR, Pacold ME, Huang Q, Clarke SM, Lam FC, Cannell IG, et al. The bromodomain protein Brd4 insulates chromatin from DNA damage signalling. Nature 2013;498:246.
26. Gadd MS, Testa A, Lucas X, Chan KH, Chen W, Lamont DJ, et al. Structural basis of PROTAC cooperative recognition for selective protein degradation. Nat Chem Biol 2017;13:514.
27. Li J, Lu Y, Akbani R, Ju Z, Roebuck PL, Liu W, et al. TCPA: a resource for cancer functional proteomics data. Nat Methods 2013;10:1046.
28. Conrad RJ, Fozouni P, Thomas S, Sy H, Zhang Q, Zhou MM, et al. The short isoform of BRD4 promotes HIV-1 latency by engaging repressive SWI/SNF chromatin-remodeling complexes. Mol Cell 2017;67:1001–12.
29. Alsarraj J, Walker RC, Webster JD, Geiger TR, Crawford NP, Simpson RM, et al. Deletion of the proline-rich region of the murine metastasis susceptibility gene Brd4 promotes epithelial-to-mesenchymal transition- and stem cell-like conversion. Cancer Res 2011;71:3121–31.
30. Mirguet O, Gosmini R, Toum J, Clément CA, Barnathan M, Brusq JM, et al. Discovery of epigenetic regulator I-BET762: lead optimization to afford a clinical candidate inhibitor of the BET bromodomains. J Med Chem 2013;56:7501–15.
31. Wang D, Qian G, Zhang H, Magliocca KR, Nannapaneni S, Amin AR, et al. HER3 targeting sensitizes HNSCC to cetuximab by reducing HER3 activity and HER2/HER3 dimerization: evidence from cell line and patient-derived xenograft models. Clin Cancer Res 2017;23:677–86.
32. Bossi P, Bergamini C, Siano M, Cossu Rocca M, Sponghini AP, Favales F, et al. Functional genomics uncover the biology behind the responsiveness of head and neck squamous cell cancer patients to cetuximab. Clin Cancer Res 2016;22:3961–70.
33. Tang Z, Li C, Kang B, Gao G, Li C, Zhang Z. GEPIA: a web server for cancer and normal gene expression profiling and interactive analyses. Nucleic Acids Res 2017;45(W1):W98–102.
34. Chung CH, Pohlmann PR, Rothenberg ML, Burkey BB, Parker J, Palka K, et al. Insulin-like growth factor-1 receptor inhibitor, AMG-479, in cetuximab-refractory head and neck squamous cell carcinoma. Head Neck 2011;33:1804–8.
35. Iida M, Bahrar H, Brand TM, Pearson HE, Coan JP, Orbuch RA, et al. Targeting the HER family with pan-HER effectively overcomes resistance to cetuximab. Mol Cancer Ther 2016;15:2175–86.
36. Stabile LP, Egloff AM, Gibson MK, Gooding WE, Ohr J, Zhou P, et al. IL6 is associated with response to dasatinib and cetuximab: phase II clinical trial with mechanistic correlatives in cetuximab-resistant head and neck cancer. Oral Oncol 2017;69(Suppl C):38–45.
37. Fury MG, Baxi S, Shen R, Kelly KW, Lipson BL, Carlson D, et al. Phase II study of saracatinib (AZD0530) for patients with recurrent or metastatic head and neck squamous cell carcinoma (HNSCC). Anticancer Res 2011;31:249–53.
38. D'Amato V, Rosa R, D'Amato C, Formisano L, Marciano R, Nappi L, et al. The dual PI3K/mTOR inhibitor PKI-587 enhances sensitivity to cetuximab in EGFR-resistant human head and neck cancer models. Br J Cancer 2014;110:2887–95.
39. Wang Z, Martin D, Molinolo AA, Patel V, Iglesias-Bartolome R, Sol Degese M, et al. mTOR Co-targeting in cetuximab resistance in head and neck cancers harboring PIK3CA and RAS mutations. J Natl Cancer Inst 2014;106:dju215.
40. Li H, Wawrose JS, Gooding WE, Garraway LA, Lui VW, Peyser ND, et al. Genomic analysis of head and neck squamous cell carcinoma cell lines and human tumors: a rational approach to preclinical model selection. Mol Cancer Res 2014;12:571–82.
41. Zawistowski JS, Bevill SM, Goulet DR, Stuhlmiller TJ, Beltran AS, Olivares-Quintero JF, et al. Enhancer remodeling during adaptive bypass to MEK inhibition is attenuated by pharmacologic targeting of the P-TEFb complex. Cancer Discov 2017;7:302–21.
42. Sakamoto T, Kawano S, Matsubara R, Goto Y, Jinno T, Maruse Y, et al. Critical roles of Wnt5a-Ror2 signaling in aggressiveness of tongue squamous cell carcinoma and production of matrix metalloproteinase-2 via ΔNp63β-mediated epithelial-mesenchymal transition. Oral Oncol 2017;69:15–25.
43. Shi J, Wang Y, Zeng L, Wu Y, Deng J, Zhang Q, et al. Disrupting the interaction of BRD4 with diacetylated twist suppresses tumorigenesis in basal-like breast cancer. Cancer Cell 2014;25:210–25.
44. Henry CE, Llamosas E, Djordjevic A, Hacker NF, Ford CE. Migration and invasion is inhibited by silencing ROR1 and ROR2 in chemoresistant ovarian cancer. Oncogenesis 2016;5:e226.
45. Adamo A, Fiore D, De Martino F, Roscigno G, Affinito A, Donnarumma E, et al. RYK promotes the stemness of glioblastoma cells via the WNT/β-catenin pathway. Oncotarget 2017;8:13476–87.
46. Cardnell R, Diao L, Wang J, Bearss D, Warner S, Fan YH, et al. An epithelial-mesenchymal transition (EMT) gene signature to predict resistance to EGFR inhibition and AXL identification as a therapeutic target in head and neck squamous cell carcinoma. J Clin Oncol 2013;31:15s (suppl; abstr 6011).
47. Klinghammer K, Otto R, Raguse JD, Albers AE, Tinhofer I, Fichtner I, et al. Basal subtype is predictive for response to cetuximab treatment in patient-derived xenografts of squamous cell head and neck cancer. Int J Cancer 2017;141:1215–21.
48. Crawford NPS, Alsarraj J, Lukes L, Walker RC, Officewala JS, Yang HH, et al. Bromodomain 4 activation predicts breast cancer survival. Proc Natl Acad Sci U S A 2008;105:6380–5.
49. Wu SY, Lee AY, Lai HT, Zhang H, Chiang CM. Phospho switch triggers Brd4 chromatin binding and activator recruitment for gene-specific targeting. Mol Cell 2013;49:843–57.
50. Wang R, Cao XJ, Kulej K, Liu W, Ma T, MacDonald M, et al. Uncovering BRD4 hyperphosphorylation associated with cellular transformation in NUT midline carcinoma. Proc Natl Acad Sci U S A 2017;114:E5352–61.
51. Hu X, Dong SH, Chen J, Zhou XZ, Chen R, Nair S, et al. Prolyl isomerase PIN1 regulates the stability, transcriptional activity and oncogenic potential of BRD4. Oncogene 2017;36:5177.
52. Fujisawa T, Filippakopoulos P. Functions of bromodomain-containing proteins and their roles in homeostasis and cancer. Nat Rev Mol Cell Biol 2017;18:246–62.
53. Shu S, Lin CY, He HH, Witwicki RM, Tabassum DP, Roberts JM, et al. Response and resistance to BET bromodomain inhibitors in triple negative breast cancer. Nature 2016;529:413–7.
54. Fong CY, Gilan O, Lam EYN, Rubin AF, Ftouni S, Tyler D, et al. BET inhibitor resistance emerges from leukaemia stem cells. Nature 2015;525:538–42.
55. Kurimchak AM, Shelton C, Duncan KE, Johnson KJ, Brown J, O'Brien S, et al. Resistance to BET bromodomain inhibitors is mediated by kinome reprogramming in ovarian cancer. Cell Rep 2016;16:1273–86.
56. Wang L, Wu X, Huang P, Lv Z, Qi Y, Wei X, et al. JQ1, a small molecule inhibitor of BRD4, suppresses cell growth and invasion in oral squamous cell carcinoma. Oncol Rep 2016;36:1989–96.